On-Chip Quantum Interference between Independent Lithium Niobate-on-Insulator Photon-Pair Sources

Robert J. Chapman,* Tristan Kuttner, Jost Kellner, Alessandra Sabatti, Andreas Maeder, Giovanni Finco, Fabian Kaufmann, and Rachel Grange

Optical Nanomaterial Group, Institute for Quantum Electronics, Department of Physics, ETH Zurich, CH-8093 Zurich, Switzerland

(Received 13 May 2024; accepted 23 April 2025; published 5 June 2025)

Generating and interfering nonclassical states of light is fundamental to optical quantum information science and technology. Quantum photonic integrated circuits provide one pathway towards scalability by combining nonlinear sources of nonclassical light and programmable circuits in centimeter-scale devices. The key requirements for quantum applications include efficient generation of indistinguishable photon-pairs and high-visibility programmable quantum interference. Here, we demonstrate a lithium niobate-on-insulator (LNOI) integrated photonic circuit that generates a two-photon path-entangled state, and a programmable interferometer for quantum interference. We generate entangled photons with $\sim 2.3 \times 10^8$ pairs/s/mW brightness and perform quantum interference experiments on the chip with $96.8 \pm 3.6\%$ visibility. LNOI is an emerging photonics technology that has revolutionized high-speed modulators and efficient frequency conversion. Our results provide a path towards large-scale integrated quantum photonics including efficient photon-pair generation and programmable circuits for applications such as boson sampling and quantum communications.

DOI: 10.1103/n2y3-2bmz

Optical quantum computers utilize nonclassical light sources, interferometric circuits, and single photon detection to perform tasks such as boson sampling that can outperform even world-leading supercomputers [1–3]. Research into quantum photonic integrated circuits has witnessed significant progress in the last years [4]. These devices miniaturize table-top experiments onto centimeter-scale chips that can run more efficiently, have the advantage of stability, and have the potential to scale far beyond their free-space optics counterparts. Today's leading integrated quantum photonics experiments use silicon and silicon-nitride waveguides that benefit from well-established nanofabrication processes and widely available foundry services for small to medium scale experiments [5]. While silicon and silicon-nitride photonics can generate photon-pairs by nonlinear four-wave-mixing [6,7], this process is inefficient compared to three-wave spontaneous parametric down-conversion (SPDC) in $\chi^{(2)}$ crystals such as lithium niobate and potassium titanyl phosphate. However, these crystals are more challenging to fabricate into scalable quantum photonic integrated circuits. As a result, the leading quantum experiments to-date still use free-space SPDC sources and circuits to prepare entangled photons [8,9] and perform postclassical boson sampling [1–3].

Lithium niobate integrated photonics is seeing a resurgence with the commercial availability of thin-film lithium-niobate-on-insulator (LNOI) wafers that can be used for high index contrast waveguides with extremely high nonlinear and electro-optic coefficients compared with bulk material [10]. LNOI photonics has made tremendous progress towards high-speed optical modulators [11] and ultra-efficient frequency conversion with periodically poled waveguides [12,13]. Despite its potential for quantum photonics, there is little progress in applying LNOI for quantum information processing beyond demonstrations of photon-pair generation [14,15] and interference of externally generated photons [16,17]. One of the key requirements for optical quantum information processing is the generation of indistinguishable photons and high-visibility interference [18]. Photon indistinguishability is crucial for generating entanglement with linear optical quantum computing [19,20], and high-visibility interference is necessary for performing high-fidelity quantum gates [21]. Integrating photon-pair generation and programmable interferometers on a single LNOI device represents a major step in quantum photonics towards and achieving an all-in-chip quantum advantage.

Here, we demonstrate a LNOI quantum photonic chip that generates indistinguishable photons in a path-entangled state, and has a programmable circuit for performing tunable quantum interference. We generate a two-photon $N00N$ state via SPDC in two identical

*Contact author: rchapman@ethz.ch

Published by the American Physical Society under the terms of the Creative Commons Attribution 4.0 International license. Further distribution of this work must maintain attribution to the author(s) and the published article's title, journal citation, and DOI.

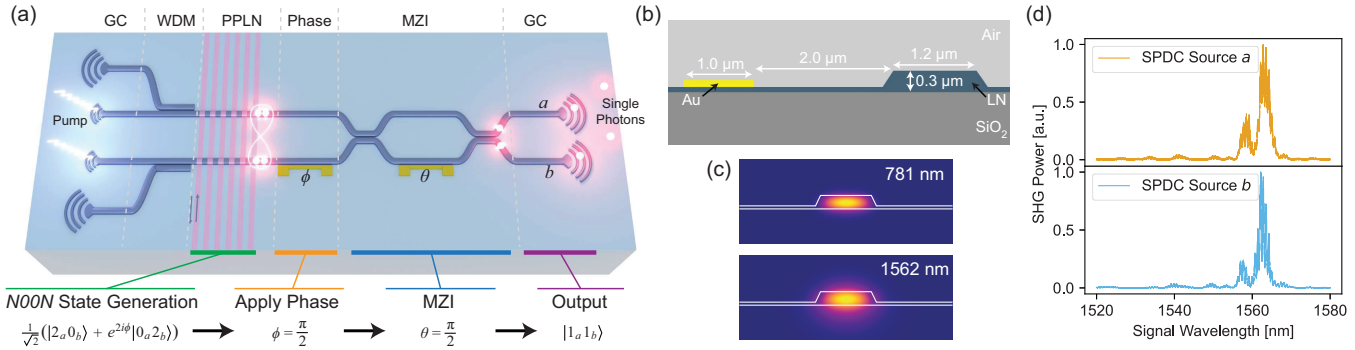


FIG. 1. LNOI quantum photonic chip. (a) The pump laser generates a path-entangled $N00N$ state across two periodically poled LNOI waveguides. The $N00N$ state phase ϕ is controlled with a thermo-optic phase shifter, and a MZI acts as a tunable beam splitter to enable quantum interference. Grating coupler (GC), wavelength division multiplexer (WDM), periodically poled LNOI (PPLN), Mach-Zehnder interferometer (MZI). (b) Cross section of the LNOI waveguide and gold thermo-optic phase shifter. (c) Optical mode at 781 and 1562 nm. (d) Second harmonic generation in the periodically poled LNOI waveguide a and b.

periodically poled LNOI waveguides, and interfere the photons with an on-chip interferometer. By modifying the phase of the $N00N$ state and the interferometer phase, we observe up to $96.8 \pm 3.6\%$ visibility quantum interference that produces bunched or antibunched photons. We generate photon pairs with an on-chip brightness of $\sim 2.3 \times 10^8$ pairs/s/mW, which is significantly higher than bulk-optics source, and verify the output two-photon state in an external Hong-Ou-Mandel experiment. Our work combines state-of-the-art quantum light sources and programmable circuits in a single device that paves the way towards large-scale quantum photonics with LNOI technology.

Results—Quantum photonic processors rely on Hong-Ou-Mandel (HOM) interference of indistinguishable photons to generate entangled states for linear optical quantum computing [19,20,22]. The HOM effect describes the bunching of photons at a 50:50 beam splitter, which generates a "$N00N$ state"—a superposition of N photons in the first mode and N photons in the second mode—with $N = 2$ for the case of two input photons such as those generated by SPDC. The $N00N$ state can be written as

$$|\psi_{N00N}\rangle = \frac{1}{\sqrt{2}}(|N_a0_b\rangle + e^{iN\phi}|0_aN_b\rangle), \tag{1}$$

where a and b indicate the mode, and ϕ is the phase with an additional factor N as a consequence of having a superposition of N photons in each waveguide. If we reverse the experiment and inject a $N00N$ state into a beamsplitter the photons will either bunch or antibunch depending on the phase that is N times more sensitive than classical interference, which is one of the key principles of quantum metrology [23]. This phenomenon can be used to separate indistinguishable photons generated by nonlinear sources into two distinct modes [7,18,24], and has been applied to prepare polarization entangled photons [25] and even $N00N$ states using a hybrid photonics approach [26].

Our LNOI quantum interference device is illustrated in Fig. 1(a). We coherently pump two periodically poled LNOI waveguides with a continuous-wave laser at 781 nm wavelength that generate photon-pairs centered at 1562 nm via type-0 SPDC. By pumping the two SPDC sources, we generate the path-entangled two-photon $N00N$ state

$$|\psi\rangle = \frac{1}{\sqrt{2}}(|2_a0_b\rangle + e^{2i\phi}|0_a2_b\rangle), \tag{2}$$

where the phase ϕ can be set with an on-chip thermo-optic phase shifter. The state $|\psi\rangle$ requires the two SPDC sources have equal photon-pair generation probability, and that the generated photons are indistinguishable. After setting the phase ϕ, the path-entangled state passes through a Mach-Zehnder interferometer (MZI) consisting of two directional couplers (H') and a phase shifter (R). A MZI acts as a tunable beam splitter with the operation $U_{\mathrm{MZI}} = H' \cdot R(\theta) \cdot H'$, where

$$H' = \frac{1}{\sqrt{2}}\begin{bmatrix} 1 & i \\ i & 1 \end{bmatrix}, \qquad R(\theta) = \begin{bmatrix} 1 & 0 \\ 0 & e^{i\theta} \end{bmatrix}, \tag{3}$$

and the phase θ is controlled by a second thermo-optic phase shifter. With $\theta = \{[(2n+1)\pi]/2\}$ for $n \in \mathbb{N}$, the MZI behaves as a 50:50 beam splitter and the chip generates the state

$$\left|\psi\left(\theta = \frac{(2n+1)\pi}{2}\right)\right\rangle = \cos(\phi)\frac{1}{\sqrt{2}}(|2_a0_b\rangle - |0_a2_b\rangle) + \sin(\phi)|1_a1_b\rangle. \tag{4}$$

This indicates that the photons will bunch with $\phi = m\pi$ for $m \in \mathbb{N}$ and will antibunch with $\phi = \{[(2m+1)\pi]/2\}$, exiting the device at separate output ports. Imbalanced

$N00N$ states and reduced photon indistinguishability lead to reduced quantum interference [27].

We fabricated our device using an x-cut LNOI wafer stack with a 300 nm lithium niobate thin film, 4.7 μm thermally grown silicon dioxide, and a 525 μm silicon handle. The cross section of the waveguide and thermo-optic phase shifter are shown in Fig. 1(b). We simulated the optical modes, shown in Fig. 1(c), using a finite element mode solver to calculate the required 2.478 μm poling period for type-0 quasi phase matching. We first deposited comb-shaped chromium electrodes on the surface of the LNOI wafer and applied voltage pulses to locally invert the lithium niobate crystal axis. The poling region is 2 mm long and the electrodes are separated by 30 μm, which is sufficient to accommodate two isolated waveguides. By increasing the separation of the poling electrodes, we could reasonably fit around 10 waveguides in a single poling region without cross coupling [12]. More details on the poling process are given in [27]. After poling, we fabricated waveguides by electron-beam lithography (EBL) of an HSQ-based mask and inductively coupled plasma reactive ion etching in argon, which leads to the typical trapezoidal waveguides observed in LNOI photonics [31]. Lastly, we deposited gold thermo-optic phase shifters via another EBL step followed by metal evaporation and lift-off. We include on-chip wavelength division multiplexers that enable us to probe the chip at both the pump and signal wavelengths. The wavelength division multiplexers are in the form of directional couplers that evanescently couple telecom wavelength light into the circuit and, because the coupling length for the pump light is far greater than that for telecom wavelength light, there is only minor loss of the pump.

We classically characterize the device to measure the phase matching of the two periodically poled waveguides and the tuning of the MZI. To characterize the phase-matching of the periodically poled waveguides, we couple a tunable telecom wavelength laser backwards through the chip and measure the up-converted second-harmonic light collected at the input grating couplers, as shown in Fig. 1(d). Both waveguides are within the same periodically poled region of the LNOI chip and we therefore expect near-identical phase matching. Indeed both waveguides have the maximum second-harmonic generation at ~1562 nm and we can compensate for any mismatch in nonlinear efficiency with the pump power in each waveguide. The second lobe observed in the up-converted signal is likely caused by variations in the lithium niobate film thickness over the length of the periodically poled region, which could be overcome by adapting the poling period along the length of the waveguide [32]. The bandwidth of the second-harmonic generation is related to the length of the periodically poled waveguide, however, the bandwidth of the generated photons is expected to be much broader due to the phase matching relation in type-0 SPDC, which could lead to reduced visibility of the on-chip

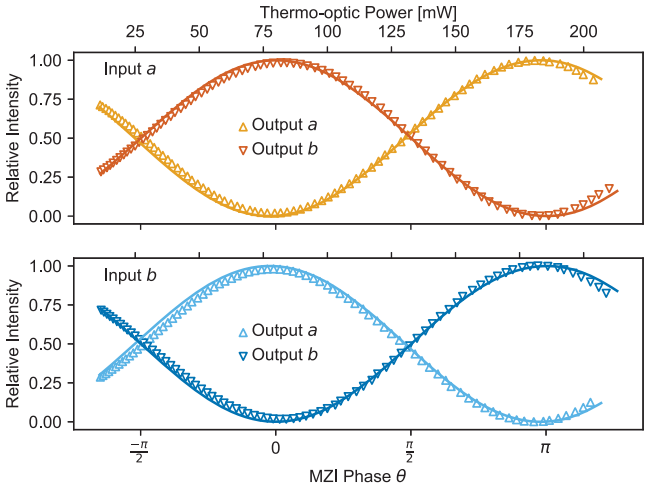


FIG. 2. MZI classical characterization. Laser light at 1562 nm is injected into one input mode of the MZI at a time. The phase θ is tuned and we monitor the optical power at both outputs of the MZI. The points represent the measurement and the line corresponds to fitting a cosine curve to the thermo-optic power.

interferometer [33]. We classically characterize the on-chip MZI by coupling laser light at 1562 nm wavelength to the chip using the on-chip wavelength division multiplexers, such that we can use grating couplers at the design wavelength. We scan the voltage of the phase shifter θ using a programmable voltage source, and measure the applied electrical power and optical output in waveguide a and b simultaneously using a v-groove fiber array and multi-channel power meter. In Fig. 2 we plot the measured optical signal for both inputs and both outputs. The visibility in the cross configuration is $> 99\%$ and in the bar configuration is $96.5 \pm 3\%$, suggesting the directional couplers have a reflectivity of $49.1 \pm 1\%$.

To generate the two-photon $N00N$ state, we inject a continuous-wave laser at 781 nm into both periodically poled waveguides simultaneously, as shown in Fig. 3(a). We use long pass filters after the chip to reject the pump, two fiber splitters and four superconducting single photon detectors to record the three two-photon states $|1_a 1_b\rangle$, $|2_a 0_b\rangle$, and $|0_a 2_b\rangle$. We scan the two on-chip phase shifters θ and ϕ, and record the coincidence rates for each state with a time tagger. In Fig. 3(b) we plot the $|1_a 1_b\rangle$ and observe peaks that correspond to antibunching when $\theta = \{[(2n+1)\pi]/2\}$ and $\phi = \{[(2m+1)\pi]/2\}$. These peaks correspond to minima in the $|2_a 0_b\rangle$ and $|0_a 2_b\rangle$ states, as shown in Figs. 3(d) and 3(f), respectively. Conversely, when $\theta = n\pi$ or $\phi = m\pi$ we observe bunching at the output of the device. To highlight the visibility of the interference we plot the three output states as a function of ϕ for $\theta = (\pi/2)$ and $\theta = \pi$ in Figs. 3(c), 3(e), and 3(g), respectively. We calculate an average visibility across all three states of $96.8 \pm 3.6\%$, suggesting that we are generating a balanced $N00N$ state, as given in Eq. (2), the photons are indistinguishable, and the linear optic circuit performs well

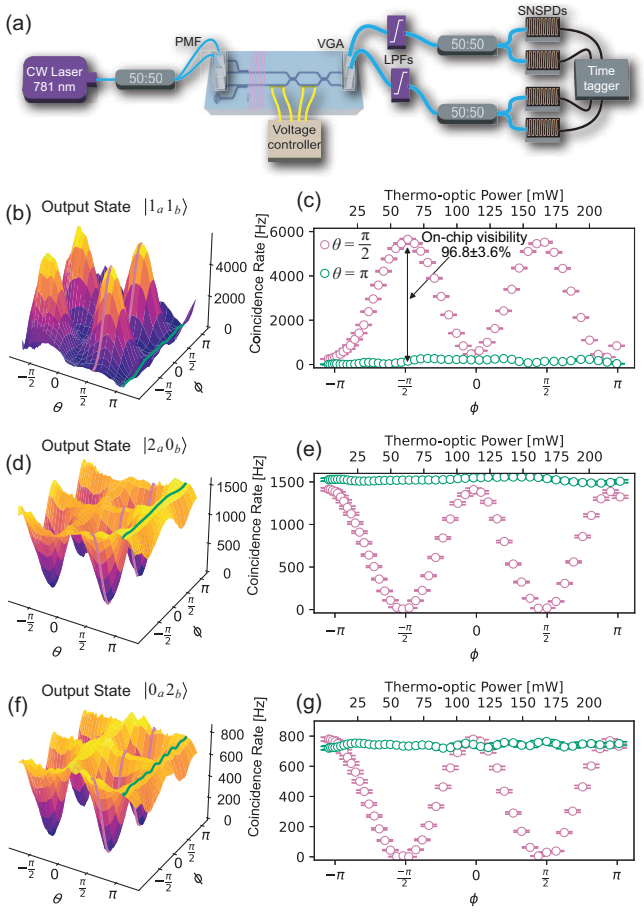


FIG. 3. On-chip quantum interference. (a) Schematic of the experiment. We pump both SPDC sources with the same laser using a 50:50 fiber beam splitter. We control each phase with a programmable voltage source. At the output we use two more 50:50 fiber beam splitters to measure all three output basis states $\{|2_a0_b\rangle, |1_a1_b\rangle, |0_a2_b\rangle\}$. Polarization maintaining fiber (PMF), V-groove fiber array (VGA), long-pass filter (LPF), superconducting nanowire single photon detector (SNSPD). (b),(c) Output probability for state $|1_a1_b\rangle$ as a function of the two phases θ and ϕ. (d),(e) Output probability for state $|2_a0_b\rangle$ as a function of the two phases θ and ϕ. (f),(g) Output probability for state $|0_a2_b\rangle$ as a function of the two phases θ and ϕ. With $\theta = \{[(2n+1)\pi]/2\}$ we observe strong bunching and antibunching, depending on the phase of the $N00N$ state ϕ. With $\theta = n\pi$ we directly observe the bunched $N00N$ state generated by SPDC.

despite the broad bandwidth expected from the SPDC source. The visibility of the quantum interference is limited by the operating bandwidth of the LNOI MZI and the spectral bandwidth of the SPDC process. Given the broad phase matching of the type-0 process, we expect the spectra of the measure SPDC photons to be limited by the bandwidth of the grating couplers. We measured the bandwidth of the LNOI MZI at the 50:50 crossing point and compared this to a fiber beam splitter, finding that the on-chip MZI deviates in reflectivity by 3.5 times less than the fiber beam splitter over the range from 1540 to 1580 nm, the bandwidth of the SPDC photon pairs [27]. This demonstrates that our LNOI MZI has a broader operating bandwidth than a commercial fiber beam splitter and should achieve a higher interference visibility with broadband photons from SPDC. Using the bandwidth of the LNOI MZI and estimated bandwidth of the out-coupled photons, we predict the maximum quantum interference visibility to be 0.978, which agrees well with our measurement. We pump the SPDC process with an estimated ~10 μW on-chip laser power and measure coincidence rates > 5800 pairs/second at the detectors with a coincidence to accidental ratio (CAR) of 55.5 ± 3.5 for source a and 79.4 ± 4.6 for source b, measured with the $g^{(2)}$ correlation function [27]. The CAR could be increased by reducing losses and pumping with a lower laser power to reduce stray light, which would also improve our quantum interference visibility. Given the output losses of ~13 dB from the grating couplers (10 dB), long-pass filters (1 dB), fiber beam splitters (1 dB) and single photon detectors (1 dB), we estimate an on-chip brightness of $\sim 2.3 \times 10^8$ pairs/s/mW. We neglect the typical waveguide loss of ~0.2 dB/cm as it adds very little to the overall loss of the device. This value is significantly higher than the leading free-space SPDC sources based on ppKTP crystals, even if we consider the broad bandwidth of our photon-pairs [34,35], and could achieve even higher values [36]. The out-coupling efficiency can be improved by reducing the grating coupler losses [37], for example, by including a back reflector [38]. We expect the maximum signal for $|2_a0_b\rangle$ and $|0_a2_b\rangle$ to be four times lower than the $|1_a1_b\rangle$ due of the nature of the state and the probabilistic separation in the fiber beam splitters. However, we record a lower coincidence rate for the $|0_a2_b\rangle$ than expected, which we attribute to misalignment between the grating and the fiber.

We finally use an off-chip HOM experiment to verify the generation of indistinguishable photons in the two output modes of the chip. To this end, we optically pump both waveguides and set the two phase shifters to $\theta = \phi = (\pi/2)$ such that the output state is $|1_a1_b\rangle$. The photons then pass through two tunable optical delay lines before interfering in a polarization maintaining fiber beam splitter. We measure the degree of photon indistinguishability by tuning the relative optical delay and recording the characteristic Hong-Ou-Mandel dip, as shown in Fig. 4. With zero time-delay, the photons bunch into one output with a visibility of $83.2 \pm 36\%$. We measure the width of the HOM dip as 71.9 ± 0.5 fs, which suggests a spectral bandwidth of the photons, after coupling into fiber, of ~50 nm. The reduced visibility can be attributed to the limited bandwidth of the commercial fiber beam splitter used in this experiment. We measured the bandwidth of the fiber beam splitter and use this to estimate the Hong-Ou-Mandel visibility given the bandwidth of the out-coupled photon pairs [27]. From this, we estimate the visibility given ideal indistinguishable photons to be 0.837, which agrees very well with our

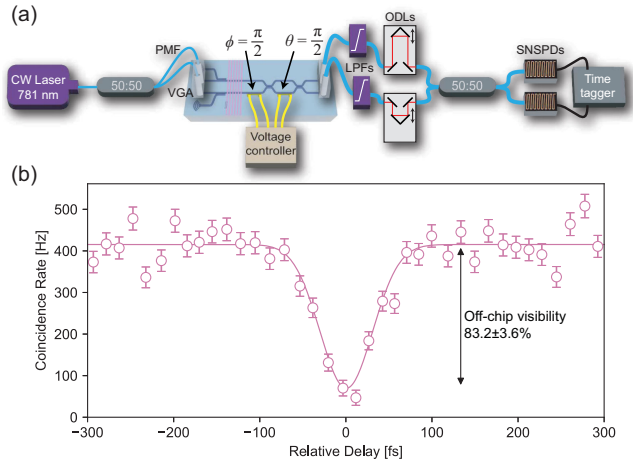


FIG. 4. Hong-Ou-Mandel interference (a) Experimental setup for measuring Hong-Ou-Mandel interference. (b) Coincidence rate with $\theta = \phi = (\pi/2)$ while scanning optical delay lines (ODLs) with the characteristic Hong-Ou-Mandel dip at zero relative delay.

experiment. Including a narrow bandpass filter between the chip and the fiber beam splitter should enable higher visibility interference, however, at the cost of photon count rate.

Discussion—Integrated photonic circuits provide a route towards scalable quantum information processing for tasks such as Gaussian boson sampling which has application in graph searches [39], vibronic spectra simulations [40], and drug discovery [41]. While significant progress has been made with silicon and silicon nitride photonics for quantum computation [5,6], these platforms have drawbacks such as a weak nonlinearity and two-photon absorption that may ultimately limit their applicability [42]. We have demonstrated that lithium niobate-on-insulator can also be applied to quantum information tasks by generating a two-photon path-entangled state and performing on-chip quantum interference in a programmable interferometer. Our device can be employed as a heralded photon source, where we utilize quantum interference to deterministically separate indistinguishable photons from the SPDC sources, as a source of $N00N$ states that surpass the shot-noise limit for phase sensitivity and can reach the Heisenberg limit, or as a platform for exploring fundamental physics, where the phase of the two-photon $N00N$ state leads to bosonic and fermionic statistics at the beam splitter. Our SPDC sources have a brightness of 2.3×10^8 pairs/s/mW for a 2 mm long waveguide and 7.7×10^6 pairs/s/nm/mW when normalizing for the photon bandwidth. This is comparable to previous LNOI works, such as [14], where a brightness of 5.6×10^7 pairs/s/nm/mW is reported for a 5 mm long waveguide, where the efficiency grows quadratically with the length. Our device also included several other photonics components such as WDMs, MZIs and grating couplers. Recently, SPDC has been demonstrated in photogalvanically (optically) poled silicon-nitride microring resonators, achieving 5.3×10^5 pairs/s/mW brightness [43]. Silicon-nitride benefits from mature nanofabrication and ultralow propagation losses of < 1 dB/m, however, the photogalvanic poling decays on a minute-long timescale, whereas periodically poled lithium niobate is stable for years. Four-wave mixing in silicon-on-insulator waveguides have been used extensively as quantum light sources [7,18,42]. In [18], a 5.2 mm long silicon waveguide is reported with 2.7×10^3 pairs/s/nm/mW^2 brightness, around 3 orders of magnitude lower than our reported device. In the context of large-scale quantum photonic integrated circuits, improving source brightness is a critical step that reduces the filtering requirements necessary to integrate single photon detectors. We elected to use thermo-optic phase shifters in this experiment, as they provide higher stability when operating at slow speeds and for fixed phase operation [44]. Utilizing slow-speed electro-optic control with lithium niobate is challenging due to dc drift leading to unstable phase shifts. Machine learning techniques have been developed to adjust the applied voltage to compensate for the dc drift and achieve stable phase shifts [45,46]. Including high-speed electro-optic switching could enable a quantum photonics platform capable of SPDC source multiplexing and feed-forward operations for quantum error correction [47]. It is now feasible to scale up our technology to many sources and large waveguide circuits for near-term quantum photonics experiments such as cluster state generation, boson sampling, and quantum enhanced metrology.

Acknowledgments—We acknowledge support for characterization of our samples from the Scientific Center of Optical and Electron Microscopy ScopeM and from the cleanroom facilities BRNC and FIRST of ETH Zurich and IBM Ruschlikon. R. J. C. acknowledges support from the Swiss National Science Foundation under the Ambizione Fellowship Program (Project No. 208707). R. G. acknowledges support from the European Space Agency (Project No. 4000137426), the Swiss National Science Foundation under the Bridge Program (Project No. 194693), and the European Research Council (Project No. 714837).

R. J. C. conceived the experiment and designed the chip. T. K., J. K., A. S., A. M., G. F., and F. K. fabricated the lithium niobate-on-insulator sample including periodic poling, lithography, etching and metal deposition. R. J. C. performed the optical measurements, data analysis, and wrote the original draft of the manuscript. R. G. supervised the project. All authors contributed to revising the manuscript.

The authors declare no competing financial or nonfinancial interests.

Data availability—Raw data and evaluation code are available from the authors upon reasonable request.

[1] H.-S. Zhong *et al.*, Quantum computational advantage using photons, Science **370**, 1460 (2020).

[2] L. S. Madsen, F. Laudenbach, M. F. Askarani, F. Rortais, T. Vincent, J. F. F. Bulmer, F. M. Miatto, L. Neuhaus, L. G. Helt, M. J. Collins, A. E. Lita, T. Gerrits, S. W. Nam, V. D. Vaidya, M. Menotti, I. Dhand, Z. Vernon, N. Quesada, and J. Lavoie, Quantum computational advantage with a programmable photonic processor, Nature (London) **606**, 75 (2022).

[3] Y.-H. Deng *et al.*, Gaussian boson sampling with pseudo-photon-number-resolving detectors and quantum computational advantage, Phys. Rev. Lett. **131**, 150601 (2023).

[4] J. Wang, F. Sciarrino, A. Laing, and M. G. Thompson, Integrated photonic quantum technologies, Nat. Photonics **14**, 273 (2020).

[5] J. C. Adcock, J. Bao, Y. Chi, X. Chen, D. Bacco, Q. Gong, L. K. Oxenløwe, J. Wang, and Y. Ding, Advances in silicon quantum photonics, IEEE J. Sel. Top. Quantum Electron. **27**, 1 (2021).

[6] J. M. Arrazola *et al.*, Quantum circuits with many photons on a programmable nanophotonic chip, Nature (London) **591**, 54 (2021).

[7] J. Bao *et al.*, Very-large-scale integrated quantum graph photonics, Nat. Photonics **17**, 573 (2023).

[8] H.-S. Zhong *et al.*, 12-photon entanglement and scalable scattershot boson sampling with optimal entangled-photon pairs from parametric down-conversion, Phys. Rev. Lett. **121**, 250505 (2018).

[9] S. Konno, W. Asavanant, F. Hanamura, H. Nagayoshi, K. Fukui, A. Sakaguchi, R. Ide, F. China, M. Yabuno, S. Miki, H. Terai, K. Takase, M. Endo, P. Marek, R. Filip, P. van Loock, and A. Furusawa, Logical states for fault-tolerant quantum computation with propagating light, Science **383**, 289 (2024).

[10] D. Zhu, L. Shao, M. Yu, R. Cheng, B. Desiatov, C. J. Xin, Y. Hu, J. Holzgrafe, S. Ghosh, A. Shams-Ansari, E. Puma, N. Sinclair, C. Reimer, M. Zhang, and M. Lončar, Integrated photonics on thin-film lithium niobate, Adv. Opt. Photonics **13**, 242 (2021).

[11] C. Wang, M. Zhang, X. Chen, M. Bertrand, A. Shams-Ansari, S. Chandrasekhar, P. Winzer, and M. Lončar, Integrated lithium niobate electro-optic modulators operating at CMOS-compatible voltages, Nature (London) **562**, 101 (2018).

[12] C. Wang, C. Langrock, A. Marandi, M. Jankowski, M. Zhang, B. Desiatov, M. M. Fejer, and M. Lončar, Ultrahigh-efficiency wavelength conversion in nanophotonic periodically poled lithium niobate waveguides, Optica **5**, 1438 (2018).

[13] J. Lu, J. B. Surya, X. Liu, A. W. Bruch, Z. Gong, Y. Xu, and H. X. Tang, Periodically poled thin-film lithium niobate microring resonators with a second-harmonic generation efficiency of 250,000%/W, Optica **6**, 1455 (2019).

[14] J. Zhao, C. Ma, M. Rüsing, and S. Mookherjea, High quality entangled photon pair generation in periodically poled thin-film lithium niobate waveguides, Phys. Rev. Lett. **124**, 163603 (2020).

[15] C. J. Xin, J. Mishra, C. Chen, D. Zhu, A. Shams-Ansari, C. Langrock, N. Sinclair, F. N. C. Wong, M. M. Fejer, and M. Lončar, Spectrally separable photon-pair generation in dispersion engineered thin-film lithium niobate, Opt. Lett. **47**, 2830 (2022).

[16] R. J. Chapman, S. Häusler, G. Finco, F. Kaufmann, and R. Grange, Quantum logical controlled-NOT gate in a lithium niobate-on-insulator photonic quantum walk, Quantum Sci. Technol. **9**, 015016 (2023).

[17] S. Babel, L. Bollmers, M. Massaro, K. H. Luo, M. Stefszky, F. Pegoraro, P. Held, H. Herrmann, C. Eigner, B. Brecht, L. Padberg, and C. Silberhorn, Demonstration of Hong-Ou-Mandel interference in an LNOI directional coupler, Opt. Express **31**, 23140 (2023).

[18] J. W. Silverstone, D. Bonneau, K. Ohira, N. Suzuki, H. Yoshida, N. Iizuka, M. Ezaki, C. M. Natarajan, M. G. Tanner, R. H. Hadfield, V. Zwiller, G. D. Marshall, J. G. Rarity, J. L. O'Brien, and M. G. Thompson, On-chip quantum interference between silicon photon-pair sources, Nat. Photonics **8**, 104 (2014).

[19] E. Knill, R. Laflamme, and G. J. Milburn, A scheme for efficient quantum computation with linear optics, Nature (London) **409**, 46 (2001).

[20] T. C. Ralph, N. K. Langford, T. B. Bell, and A. G. White, Linear optical controlled-NOT gate in the coincidence basis, Phys. Rev. A **65**, 062324 (2002).

[21] C. Taballione, M. C. Anguita, M. d. Goede, P. Venderbosch, B. Kassenberg, H. Snijders, N. Kannan, W. L. Vleeshouwers, D. Smith, J. P. Epping, R. v. d. Meer, P. W. H. Pinkse, H. v. d. Vlekkert, and J. J. Renema, 20-mode universal quantum photonic processor, Quantum **7**, 1071 (2023).

[22] C. K. Hong, Z. Y. Ou, and L. Mandel, Measurement of subpicosecond time intervals between two photons by interference, Phys. Rev. Lett. **59**, 2044 (1987).

[23] J. P. Dowling, Quantum optical metrology—the low-down on high-N00N states, Contemp. Phys. **49**, 125 (2008).

[24] H. Jin, F. M. Liu, P. Xu, J. L. Xia, M. L. Zhong, Y. Yuan, J. W. Zhou, Y. X. Gong, W. Wang, and S. N. Zhu, On-chip generation and manipulation of entangled photons based on reconfigurable lithium-niobate waveguide circuits, Phys. Rev. Lett. **113**, 103601 (2014).

[25] L. Sansoni, K. H. Luo, C. Eigner, R. Ricken, V. Quiring, H. Herrmann, and C. Silberhorn, A two-channel, spectrally degenerate polarization entangled source on chip, npj Quantum Inf. **3**, 1 (2017).

[26] S. Atzeni, A. S. Rab, G. Corrielli, E. Polino, M. Valeri, P. Mataloni, N. Spagnolo, A. Crespi, F. Sciarrino, and R. Osellame, Integrated sources of entangled photons at the telecom wavelength in femtosecond-laser-written circuits, Optica **5**, 311 (2018).

[27] See Supplemental Material at http://link.aps.org/supplemental/10.1103/n2y3-2bmz for effects impacting *N*00*N* state fidelity, information on the periodic poling process, details of the experimental setup and information

on the MZI bandwidth and loss, which includes Refs. [28–30].

[28] E. Lomonte, F. Lenzini, and W. H. P. Pernice, Efficient self-imaging grating couplers on a lithium-niobate-on-insulator platform at near-visible and telecom wavelengths, Opt. Express **29**, 20205 (2021).

[29] A. Sabatti, J. Kellner, F. Kaufmann, R. J. Chapman, G. Finco, T. Kuttner, A. Maeder, and R. Grange, Extremely high extinction ratio electro-optic modulator via frequency upconversion to visible wavelengths, Opt. Lett. **49**, 3870 (2024).

[30] R. Nehra, R. Sekine, L. Ledezma, Q. Guo, R. M. Gray, A. Roy, and A. Marandi, Few-cycle vacuum squeezing in nanophotonics, Science **377**, 1333 (2022).

[31] F. Kaufmann, G. Finco, A. Maeder, and R. Grange, Redeposition-free inductively-coupled plasma etching of lithium niobate for integrated photonics, Nanophotonics **12**, 1601 (2023).

[32] P.-K. Chen, I. Briggs, C. Cui, L. Zhang, M. Shah, and L. Fan, Adapted poling to break the nonlinear efficiency limit in nanophotonic lithium niobate waveguides, Nat. Nanotechnol. **19**, 44 (2024).

[33] F. Graffitti, J. Kelly-Massicotte, A. Fedrizzi, and A. M. Brańczyk, Design considerations for high-purity heralded single-photon sources, Phys. Rev. A **98**, 053811 (2018).

[34] M. V. Jabir and G. K. Samanta, Robust, high brightness, degenerate entangled photon source at room temperature, Sci. Rep. **7**, 12613 (2017).

[35] S. Meraner, R. Chapman, S. Frick, R. Keil, M. Prilmüller, and G. Weihs, Approaching the Tsirelson bound with a Sagnac source of polarization-entangled photons, SciPost Phys. **10**, 017 (2021).

[36] G.-T. Xue, Y.-F. Niu, X. Liu, J.-C. Duan, W. Chen, Y. Pan, K. Jia, X. Wang, H.-Y. Liu, Y. Zhang, P. Xu, G. Zhao, X. Cai, Y.-X. Gong, X. Hu, Z. Xie, and S. Zhu, Ultrabright multiplexed energy-time-entangled photon generation from lithium niobate on insulator chip, Phys. Rev. Appl. **15**, 064059 (2021).

[37] I. Krasnokutska, R. J. Chapman, J.-L. J. Tambasco, and A. Peruzzo, High coupling efficiency grating couplers on lithium niobate on insulator, Opt. Express **27**, 17681 (2019).

[38] B. Chen, Z. Ruan, X. Fan, Z. Wang, J. Liu, C. Li, K. Chen, and L. Liu, Low-loss fiber grating coupler on thin film lithium niobate platform, APL Photonics **7**, 076103 (2022).

[39] S. Yu *et al.*, A universal programmable Gaussian boson sampler for drug discovery, Nat. Comput. Sci. **3**, 839 (2023).

[40] J. Huh, G. G. Guerreschi, B. Peropadre, J. R. McClean, and A. Aspuru-Guzik, Boson sampling for molecular vibronic spectra, Nat. Photonics **9**, 615 (2015).

[41] S. Sempere-Llagostera, R. B. Patel, I. A. Walmsley, and W. S. Kolthammer, Experimentally finding dense subgraphs using a time-bin encoded Gaussian boson sampling device, Phys. Rev. X **12**, 031045 (2022).

[42] J. W. Silverstone, D. Bonneau, J. L. O'Brien, and M. G. Thompson, Silicon quantum photonics, IEEE J. Sel. Top. Quantum Electron. **22**, 390 (2016).

[43] B. Li, Z. Yuan, J. Williams, W. Jin, A. Beckert, T. Xie, J. Guo, A. Feshali, M. Paniccia, A. Faraon, J. Bowers, A. Marandi, and K. Vahala, Down-converted photon pairs in a high-Q silicon nitride microresonator, Nature (London) **639**, 922 (2025).

[44] A. Maeder, F. Kaufmann, D. Pohl, J. Kellner, and R. Grange, High-bandwidth thermo-optic phase shifters for lithium niobate-on-insulator photonic integrated circuits, Opt. Lett. **47**, 4375 (2022).

[45] A. Youssry, R. J. Chapman, A. Peruzzo, C. Ferrie, and M. Tomamichel, Modeling and control of a reconfigurable photonic circuit using deep learning, Quantum Sci. Technol. **5**, 025001 (2020).

[46] A. Youssry, Y. Yang, R. J. Chapman, B. Haylock, F. Lenzini, M. Lobino, and A. Peruzzo, Experimental graybox quantum system identification and control, npj Quantum Inf. **10**, 1 (2024).

[47] S. Saravi, T. Pertsch, and F. Setzpfandt, Lithium niobate on insulator: An emerging platform for integrated quantum photonics, Adv. Opt. Mater. **9**, 2100789 (2021).